

Lattice QCD with chemical potential: Evading the fermion-sign problem

SOURENDU GUPTA

Department of Theoretical Physics, Tata Institute of Fundamental Research,
Homi Bhabha Road, Mumbai 400 005, India
E-mail: sgupta@theory.tifr.res.in

Abstract. Since the turn of the millennium there has been tremendous progress in understanding QCD at finite chemical potential, μ . Apart from qualitative results obtained using models, and exact results at very large μ obtained in weak coupling theory, there has been tremendous progress in getting exact and quantitative results from lattice simulations. I summarize the status of lattice QCD at finite chemical potential – locating the critical end-point in the QCD phase diagram, predicting event-to-event fluctuation rates of conserved quantities, and finding the rate of strangeness production.

Keywords. Quantum chromodynamics; Fermion-sign problem; critical end-point.

PACS Nos 11.15.Ha; 12.38.Gc; 12.38.Mh; 25.75.Nq

1. Preliminaries

In the last few years there has been a burst of work in elucidating the phase structure of QCD, especially the remarkable variety of phases and phase transitions at small temperature, T , and large baryon chemical potential, μ . Among the new results, the most dependable are from weak-coupling analysis, valid at very large μ , and lattice results, valid at small μ .

Excitations around the filled Fermi sea of quarks interact with the strength of the running coupling determined by the large scale μ . Consequently, the results are dependable whenever μ is sufficiently large. The main result is that there is an attractive interaction between particle hole pairs leading to colour superconductivity [1]. Gap equations have been set up and solved and the line of phase transition between hot quark matter and cold colour superconducting matter has been found [2]. The most favoured pairing pattern for 2 + 1 quark flavours (shorthand for two light and one heavier flavour) in QCD is the so-called colour-flavour locked (CFL) phase [3].

Models have been used to continue the phase diagram towards smaller μ . The mass differences between the strange and light quarks give interesting changes in the phase diagram at smaller μ [4]. Along the $\mu = 0$ line hard predictions are available from lattice QCD. It is known that at finite quark masses there is a cross-over (not a

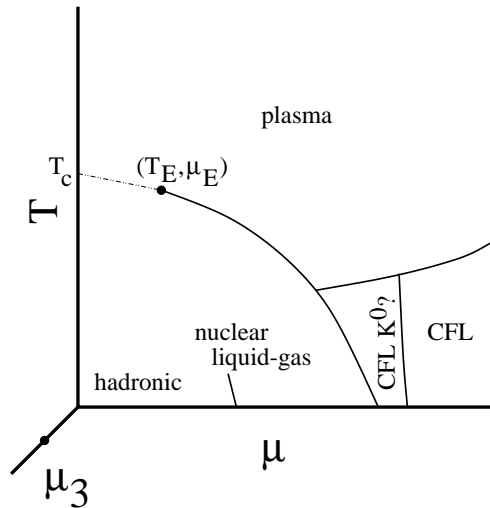


Figure 1. Part of the conjectured phase diagram of QCD for 2+1 flavours, when weak and electromagnetic interactions are switched off, and the quark masses have their physical value. Every solid line denotes a first-order phase transition. Every open end of such a line is a critical end-point. The dotted lines denote cross-overs – along the $\mu = 0$ axis, there is a rapid cross-over between the hadronic and plasma phases at T_c . An important question is whether the critical end-point (T_E, μ_E) is close enough to the $\mu = 0$ axis to be visible at the RHIC. The other critical end-point at much smaller temperature, for the nuclear liquid–gas transition has possibly been observed [11]. At large μ , the transition line between the plasma and CFL phases has no end-point. The CFL K^0 phase is characterized in [4]. Along the μ_3 axis, there is a critical point for charged pion condensation at $\mu_3 = m_\pi$ [12]. In the phase diagram for $N_f = 2$, the CFL phases are replaced by a different colour superconducting phase without changing the character of the phase diagram at low μ . For $N_f = 3$ and higher, the phase diagram is quite different.

phase transition) from the hadronic phase to the hot quark matter phase. Putting all this information together, one gets the conjectured phase diagram shown in figure 1. In this talk I shall focus on recent attempts to determine the location of the critical end-point directly through lattice computations. I shall restrict my attention to the work done in QCD with 2 or 2 + 1 flavours, for which the critical end-point exists.

It is well-known that a quantum theory with unequal numbers of fermions and anti-fermions has a ‘sign problem’, i.e., the Euclidean partition function is not positive definite. In essence the problem arises from the fact that fermions are anti-symmetric under exchange. This problem has prevented widespread use of the Monte Carlo method for the exploration of the phase diagram of many models of physical interest in a variety of fields, ranging from the Hubbard model and applications to high- T_c superconductivity to QCD at finite baryon density. The exciting development in the last three years has been that not only one, but three different methods have been developed which can be used to bypass the sign problem

[5–10]. I will outline the results obtained by these means on the phase diagram and related physics.

It is perhaps useful to mention here a few issues which will not be discussed later. First, that in QCD, where flavour symmetry is exact, it is possible to put an independent chemical potential for each quark flavour. QCD at finite iso-vector chemical potential ($\mu_3 = \mu_u = -\mu_d$) suffers from no sign problem, and can be computed directly. However, when weak interactions are switched on only the baryon and electric charge remain conserved, and only these two chemical potentials remain meaningful. Second, the new methods are not full solutions to the sign problem, but allow us to bypass it in a certain part of the phase diagram. The superconducting phases of QCD still remain out of reach of the present lattice methods. Unfortunately, therefore, quantitative statements about the differences between nuclear and quark matter in the core of compact stars still remain out of reach of exact theory.

2. The new lattice techniques

The lattice results are based on three new techniques, all developed in the last two years. One of these techniques, the use of imaginary chemical potential [9,10], is specific to QCD-like theories where an imaginary chemical potential behaves as an extra $U(1)$ piece in the gauge group, and hence leads to a formulation without the sign problem. An appropriate analytic continuation can then allow one to find the location of the critical end-point.

The other two formulations are more general, and can be directly carried over to other physical systems where the sign problem exists; these are the reweighting method [5,6] and the Taylor series expansion method [7,8]. They are subject to different kinds of uncertainties. I will illustrate them here with an application to a directly solvable problem – the evaluation of Gaussian integrals:

$$\bar{x}(s) = \frac{1}{\sqrt{2\pi}} \int_{-\infty}^{\infty} dx e^{-(x-s)^2/2}. \quad (1)$$

The exact solution is $\bar{x}(s) = s$. Although there is no sign problem here, one can use the above methods to generate $\bar{x}(s)$ numerically.

The reweighting method consists of rewriting the problem as

$$\bar{x}(s) = \frac{1}{\sqrt{2\pi}} \int_{-\infty}^{\infty} dx w(x, s) e^{-x^2/2} = \frac{\langle xw(x, s) \rangle}{\langle w(x, s) \rangle}, \quad (2)$$

where $w(x, s) = \exp(2sx - s^2)/2$, and angular brackets denote an average over the Gaussian weight $dx \exp(-x^2/2)$. In reweighting, this weight is sampled by a Monte Carlo technique, and the dependence on s generated by $w(x, s)$.

Such reweighting techniques have been suggested earlier as a means of getting round the sign problem [13]. However, the sign problem then manifests itself as large cancellations (and consequent large errors) in the determination of the denominator, $\langle w \rangle$. The approach of [5] hopes to avoid this problem by a clever choice of correlated paths of reweighting in the $T-\mu$ plane. This cannot remove all the problems of

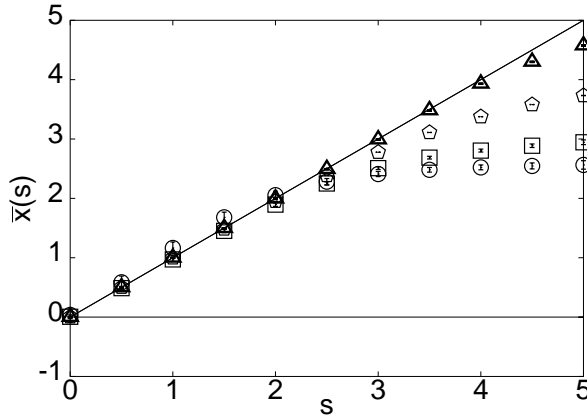


Figure 2. Reweighting the Gaussian with different statistics (circle: 100, square: 1000, pentagon: 10^5 and triangle: 10^7). The naive error bars shown here are clearly too optimistic, as is clear on comparing with the exact result (thick diagonal line). Note that the extra range of s gained grows at best logarithmically with the statistics.

course, as one can see by replacing $\langle w \rangle$ in eq. (2) by its known value $\sqrt{2\pi}$. The results of reweighting of simulations with different statistics is compared with the exact result in figure 2. As one can see, the extent by which one can extrapolate in s grows logarithmically with the statistics.

This exponential barrier is generic for reweighting, and is due to the fact that no matter how large the statistics, there will be some range of configurations which must have exponentially small weight (guaranteed by the fact that thermodynamic fluctuations are generically Gaussian) and therefore will not be sampled very well. As one reweights, configurations which are badly sampled will eventually dominate the averaging and destroy the reweighting (see figure 3). Clearly, an absolute upper bound on reweighting, s_{lim} , is obtained for a given statistics, N_s , when the maximum of the reweighted distribution is at a point where the original distribution had only one event, i.e.,

$$N_s P(s_{\text{lim}}) = 1 \quad \text{and} \quad s_{\text{lim}}^{\text{Gaussian}} = \sqrt{2\sigma} \log \left(\frac{N_s}{\sqrt{2\pi\sigma}} \right). \quad (3)$$

The equation at the left is valid for all distributions, whereas the expression on the right is correct for a Gaussian of variance σ . The actual extent to which one can extrapolate by reweighting is usually much smaller [14]. An improved analysis of errors in reweighting [15], as displayed in figure 4 also reveals the exponential barrier. For the unit Gaussian with statistics of $N_s = 10^3$, we expect, $s_{\text{lim}}^{\text{Gaussian}} = 8.47$. As expected, this is far larger than the analysis shown in figure 4, from which it seems difficult to extrapolate beyond $s = 2$.

One way to approach the Taylor expansion method is to simply expand the weight factor $w(x, s)$ in a Taylor series in s , as in [6]. However, this does not necessarily lead to a better controlled expansion. The real improvement comes from taking the Taylor expansion of an expectation value [7], in this case \bar{x} . This allows the

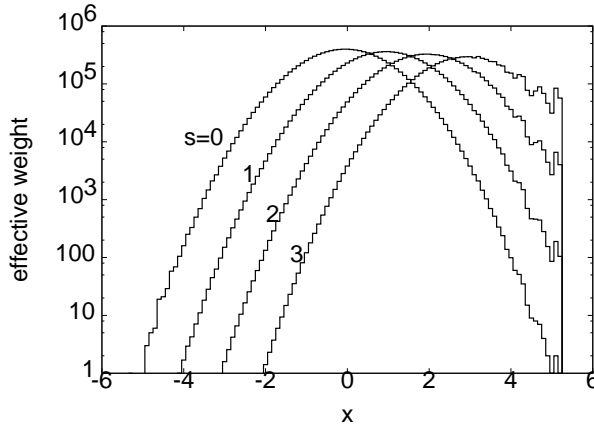


Figure 3. The histograms generated by reweighting of that obtained by direct Monte Carlo simulations at $s = 0$ using statistics of 10^6 . The distance to which reweighting is accurate depends on the logarithm of the statistics and the width of the distribution.

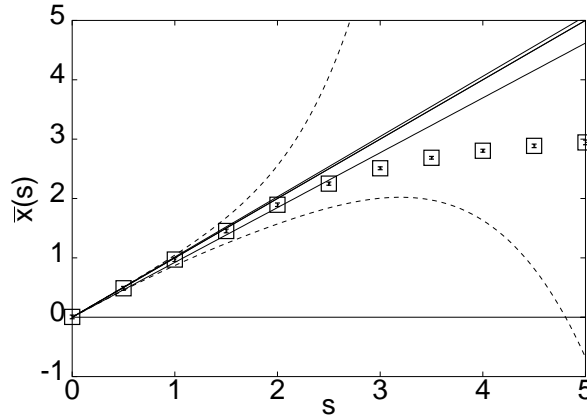


Figure 4. Improved estimate of one sigma errors in reweighting using 1000 sample points (dashed line). Also shown is the error band for the extrapolation using a Taylor expansion based on the same statistics (full line).

Monte Carlo to solve more of the problem by using all the symmetries at hand, and, through importance sampling, also determine enough of the weight to improve the extrapolation. In fact, the symmetries of the problem allow us to drop all the even order terms in the expansion, leaving us with the remaining coefficients:

$$\begin{aligned}
 1!t_1 &= [x^2], \\
 3!t_3 &= [x^4] + 3 [x^2] ([x^2] - 1), \\
 5!t_5 &= [x^6] + [x^4] (15 [x^2] - 10) + 15 [x^2] ([x^2] - 1)^2,
 \end{aligned} \tag{4}$$

where t_i is the Taylor coefficient of the i th order in the expansion of \bar{x} , and square brackets denote cumulants, i.e., the connected parts of moments. For the Gaussian

problem at hand, all cumulants except $[x^2]$ are zero. The results of the Taylor expansion are shown in figure 4.

The Taylor expansion becomes statistically unreliable when the error in some term dominates the expansion. The coefficient itself is always of order $\langle x^n \rangle / n!$, and its error dominates for a limiting order, n_* , such that

$$N_e P \left(\left\{ \frac{\langle x^{n_*} \rangle}{n_*!} \right\}^{1/n_*} \right) = 1. \quad (5)$$

For a Gaussian distribution, the limiting order $n_* \propto \log^2 N_s$. However, the limiting value, s^{lim} , is independent of n_* , since $s^{\text{lim}} = R$, where R is the radius of convergence of the series. This R in turn can be determined from the Taylor expansion with an error that is well-behaved for $n < n_*$. The method would fail if the series is badly behaved and asymptotic results for R cannot be obtained with $n < n_*$. For the example here, or for the high temperature phase of QCD, where the series has an infinite radius of convergence [7], there is no threshold where the expansion breaks down, as is clearly visible in figure 4.

A Taylor series expansion of the pressure in terms of μ along lines of constant T ,

$$\frac{1}{V} Z(T, \mu) = P(T, \mu) = P(T, 0) + \sum_i \frac{\chi_{2i}}{2i!} \mu^{2i} \quad (6)$$

contains only the even order terms due to CP invariance [16]. It breaks down at the critical end-point, which is the radius of convergence of the series. The statistical errors in the estimate of the critical end-point are well-behaved as a function of the statistics. Hence the Taylor expansion method seems to be very well-suited for the determination of the critical end-point.

This estimate can be made through the ratio test for convergence of a series:

$$\mu_n = \sqrt{(n+1)(n+2) \frac{\chi_n}{\chi_{n+2}}} \quad (7)$$

where an estimator of the radius of convergence, μ_* , is the limit of μ_n as n tends to infinity. The series converges if and only if $\mu \leq \mu_*$ [7,8].

I return briefly to a discussion of the technique of lattice simulation at imaginary chemical potential and its analytic continuation to real chemical potential. Theoretically the most well-founded method for the analytic continuation is through the Taylor expansion of the pressure, as in eq. (6). This was used in [9] and explored further in [19]. In the latter, the case of $SU(2)$ colour group was examined, since the action remains positive-definite even for real chemical potential. It was found that a small number of coefficients could be extracted with sufficient precision to perform the analytic continuation.

It is clear that the system for imaginary μ (i.e., $\mu^2 < 0$) is not physical [20]. A complication in this method is that simulations at imaginary chemical potential can see multiple vacua which are not physical, and hence be constrained by other nearby singularities. It remains to be seen whether this method is accurate enough to yield the position of the critical end-point.

3. The critical end-point in QCD

These are early days for the determination of the critical end-point in QCD. Several independent estimates are now available at the same lattice spacing $a = 1/4T_c$ with degenerate u and d quark masses such that $m_\rho/T_c \approx 5$. Two of these computations [8,21] are performed with two flavours of light dynamical quarks and the others [5,22] add a heavier dynamical quark with bare quark mass $m_s/m_u = 8$. Since the parameters in the staggered quark simulations [5,21] are related in such a way that $m_\pi/T_c = 1.6$ and $m_\pi/m_\rho = 0.3$ [5,23], it is clear that the heavier (strange) quark of [5] has little influence on the scale. One consequence of this is that the observation in [23] that lattice artifacts are strong, since the nucleon mass is too heavy, with $m_N/m_\rho = 1.8$, extends to the simulation of [5]. With the P4 improved staggered quark action used in [8] the above value of m_ρ/T_c is obtained for $m_\pi/m_\rho = 0.70$ [24], implying that the quark mass is large. It is clear that the continuum results for the critical end-point are yet to come: the current excitement is that it has been reduced to an economic problem of buying enough computer time.

The first results for the critical end-point for $2 + 1$ flavours were obtained for staggered quarks with two light flavours of $m/T_c = 0.1$ and 1 heavier flavour of $m/T_c = 0.8$ on 4×4^3 , 4×6^3 and 4×8^3 lattices [5]. The quark masses are rather high, as evidenced by the fact that $m_\pi/T_c \approx 1.6$ instead of the expected value of about unity, and $m_\pi/m_\rho \approx 0.3$, almost twice as large as in the physical world. Even though the pion mass is large, the spatial sizes are small when expressed in units of the relevant physical quantity that controls the dominant finite volume effects, i.e., the pion Compton wavelength. Subject to all these caveats, the estimate of the critical point reported by these authors is $T_E = 160 \pm 3.5$ MeV and $\mu_E = 725 \pm 35$ MeV.

The scale in [5] is set by a determination of $T_c = 172 \pm 3$ MeV. This gives $T_E/m_\rho = 0.191 \pm 0.006$ and $\mu_E/m_\rho = 0.86 \pm 0.05$. Since the scale of T_c is likely to be set by the rho meson, and that of μ_E by the nucleon, it is useful to know that $\mu_E/m_N = 0.49 \pm 0.03$. Then setting the scale by the physical nucleon mass, one would get $\mu_E = 460 \pm 25$ MeV. Thus, the scale uncertainty in the result is much greater than the statistical errors quoted.

It is also interesting to see that $T_E/T_c = 0.93 \pm 0.03$. Possible systematic effects in the error remain to be investigated. One expects the largest effect to come from finite volume rounding and shift in the critical point. For example, using the known shift in the Wilson coupling for the quenched theory [25], it turns out that $\Delta T_c/T_c = 0.03$ on comparable lattice sizes.

A recent update brought the quark mass down [22]; with $m_\pi/m_\rho = 0.18$, in agreement with its physical value. The strange quark mass was tuned to give $m_\pi/m_K \simeq 0.3$, which is also realistic. However, the cut-off remained $a = 1/4T_c$ and m_ρ/T_c increased marginally. Nor were the spatial volumes (measured in physical units) increased in these computations. The critical end-point was identified to lie at $T_E = 162 \pm 2$ and $\mu_E = 360 \pm 40$. Using the estimates of T_c and m_ρ presented, this corresponds to $T_E/m_\rho = 0.184 \pm 0.003$ and $\mu_E/m_\rho = 0.41 \pm 0.05$.

Taylor expansions have been used with both staggered quarks [7,21] and Symanzik improved P4 quarks [8] with two flavours of light degenerate quarks. In [21], the bare quark mass, $m/T_c = 0.1$, corresponds to $m_\pi/T_c \simeq 1.6$ [23], the

Table 1. Summary of critical end-point determinations. The lattice spacing is $a = 1/4T_c$. L is the spatial size of the lattice and Lm_π is the size in units of the pion Compton wavelength. The ratio m_π/m_K sets the scale of the strange quark mass. As the mass scales indicate, the lattice spacings and u and d quark masses of [5] and [21] are comparable. The number in brackets indicate the statistical errors on the least significant digit.

Lm_π	m_ρ/T_c	m_π/m_ρ	m_N/m_ρ	Flavours	m_π/m_K	μ_E/T_E	Reference
1.57–3.14	5.12 (8)	0.307 (6)	?	2+1	?	1.51 (8)	[5]
1.49–2.99	5.372 (5)	0.185 (2)	?	2+1	0.282 (4)	0.74 (8)	[22]
4.18–10.04	5.4 (2)	0.31 (1)	1.8 (2)	2	–	1.3–2.0	[21]
15.33	5.5 (1)	0.70 (1)	?	2	–	?	[8]

spatial sizes are varied to lie between about 4 and 10 times the pion Compton wavelengths, and all Taylor coefficients up to the eighth order are computed. In [8], the bare quark mass $m/T_c = 0.4$ corresponds to $m_\pi/T_c \simeq 4$, the spatial size is about 15 pion Compton wavelengths, and Taylor coefficients up to the fourth order are computed.

In [7] it was found that the radius of convergence of the Taylor series for the pressure was large (possibly infinite) in the plasma phase of quenched QCD in the continuum limit. This result was reproduced at finite lattice spacing in the two-flavour theory [21]. On lowering the temperature, it was found that in the region between T_c and $0.95T_c$ there is a cross-over to a finite radius of convergence. At $T/T_c = 0.95$, the radius of convergence is estimated to be 0.710 ± 0.002 (for $Lm_\pi \simeq 4.2$) and 0.500 ± 0.004 (for $Lm_\pi \simeq 6.7$). In the infinite volume limit, it is estimated that $\mu_E/T_E \approx 1.3-2$, which is in rough agreement with the results due to reweighting. However, the finite volume effects seen here could imply that the results of the critical end-point estimate for 2 + 1 flavours in the infinite volume limit could easily move towards significantly smaller μ_E .

A summary of these discussions is given in table 1 [26]. The state of the art needs to be improved in three ways. First, finite volume effects need to be explored in order to check whether the putative end-point is really *critical*. The first steps in this direction have been taken in [21]. Second, smaller quark masses have to be used in order to check what happens when the hadron masses are physical. Again, the first step in this direction has been taken [22]. Finally, the continuum limit needs to be taken in order to make contact with experiment.

4. Physics at small μ

The ability to compute at finite chemical potential opens up new physics channels where data from RHIC and other heavy-ion facilities can be compared with theoretical predictions. Some of the new physics that has been explored are event-to-event fluctuations (of conserved quantities such as baryon number, charge and strangeness), the equation of state and total strangeness production rates.

4.1 Quark number susceptibilities

The relation between quark number susceptibilities and event-to-event fluctuations of conserved quantities was set out in [27]. Computations of the quark number susceptibilities at temperatures well above T_c were first performed in a quenched lattice computation [28] and extrapolated to the continuum [29]. Perturbative estimates using the 2PI skeleton resummation [30] and dimensional reduction [31] agree with these results. In figure 5 we show the temperature dependence of the quark number susceptibility at lattice spacing $a = 1/4T$ using 2 flavours of staggered quarks [21]. A comparison with the quenched theory shows that quenching artifacts are small in the high temperature limit. A speciality of these computations is that the quark mass is adjusted to take care of the running due to changing lattice spacing so that physical masses are fixed to $m_\rho/T_c = 5.4$.

Similar computations have been performed with 2 flavours of P4 improved staggered quarks [8] as well as 2+1 and 3 flavours of Asqtad improved staggered quarks [33]. In the latter, the running of the quark mass is taken care of by adjusting it keeping $m_\pi/m_\rho = 0.672$ for $N_f = 3$ and $m_\pi/m_\rho = 0.392$ when $m_{u,d}/m_s = 0.2$. This was done while the lattice spacing was varied between $1/4T$ and $1/8T$ with T running from approximately $0.75T_c$ to $1.5T_c$. Qualitatively, the results are very similar to those shown in figure 5, although there are quantitative differences due to the differences in m_π/m_ρ or the number of active flavours. The computations of [33] show a large change in going from $a = 1/4T$ to $a = 1/6T$, followed by little movement in decreasing a to $1/8T$. Additionally, the results indicate that the continuum limit for $T > T_c$ may be close to that in the quenched theory [29].

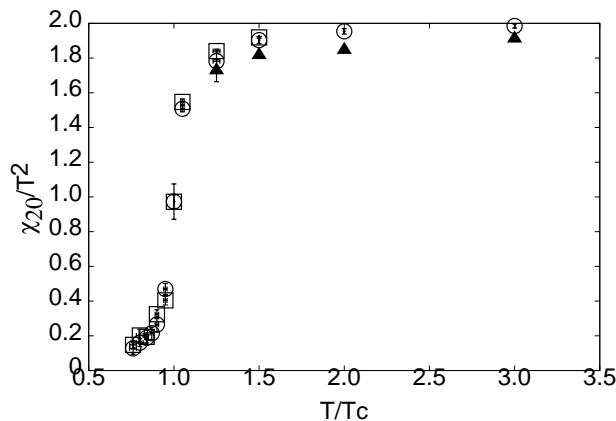


Figure 5. The quark number susceptibility χ_{20}/T^2 as a function of T at lattice spacing $a = 1/4T$. The full temperature range is covered for two flavours of staggered quarks with bare quark mass fixed to give $m_\pi/T_c = 1.6$ with spatial box size of 4 pion Compton wavelengths (circles) and 6.4 pion Compton wavelengths (boxes). In the high temperature phase the results are comparable with those from quenched theory at the same lattice spacing (triangles) [28]. There are attempts to describe the data below T_c in terms of an ideal resonance gas [32].

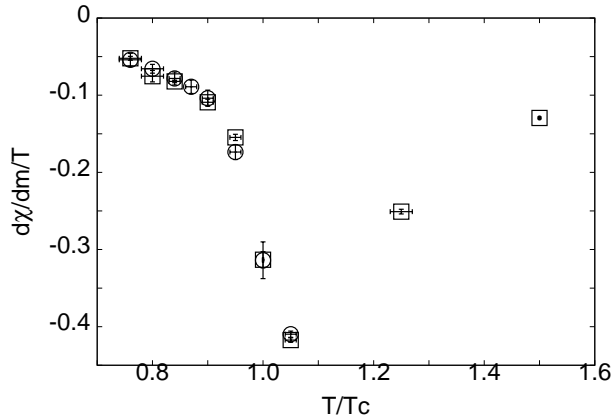


Figure 6. The bare quark-mass dependence of the quark number susceptibility χ_{20}/T^2 as a function of T at lattice spacing $a = 1/4T$. The full temperature range is covered for two flavours of staggered quarks with bare quark mass fixed at $m/T_c = 0.1$ (independent of the lattice spacing) in order to give $m_\pi/T_c = 1.6$ with spatial box size of 4 pion Compton wavelengths (circles) and 6.4 pion Compton wavelengths (boxes). Note that the mass shift is small: halving the quark mass changes χ_{20}/T^2 in figure 5 by less than the error bars at almost all T .

The quark mass dependence of the quark number susceptibility which is required to connect all the different computations is related to an interesting physical quantity by a Maxwell relation, i.e., an equality between two different physical interpretations of a mixed derivative obtained by interchanging the orders of the derivatives. When a Taylor expansion of the quark condensate is written down, the coefficient of the linear term is seen to vanish for the flavour singlet condensate. The Maxwell relation for the coefficient of the quadratic term is:

$$\frac{\partial^2 \langle \bar{\psi}\psi \rangle}{\partial \mu^2} = \frac{\partial \chi_{20}}{\partial m}. \quad (8)$$

The bare derivative is shown in figure 6 in the theory with two flavours of dynamical staggered quarks as a function of temperature. Renormalisation and the continuum limit were investigated in the quenched theory [34], and it was shown that the relatively large value of the derivative seen for $T > T_c$ in figure 6 is a lattice artifact. In the continuum this derivative vanishes. No investigation of this kind has been performed yet below T_c .

4.2 The equation of state

The equation of state can be used and tested in the analysis of collective flow arising in heavy-ion collisions. In the high temperature phase of QCD where quenching artifacts are small, the continuum limit has been taken in quenched QCD [7]. In heavy-ion experiments at RHIC and the CERN-SPS, the chemical potential has

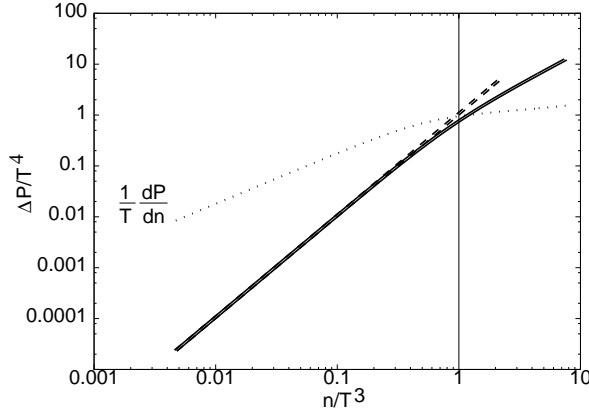


Figure 7. The equation of state in the continuum limit at finite chemical potential for $T = 2T_c$ with the leading term only (dashed line), and the first two terms (full line) of the Taylor series. The band shows the $1\text{-}\sigma$ error due to statistical errors in the susceptibilities. The EOS at $1.5T_c$ and $3T_c$ are indistinguishable at this scale. The dotted line is the response function $\partial(P/T^4)/\partial(n/T^3)$ at fixed T .

been extracted from analysis of hadronic yields [35]. At SPS energies, where $\mu/T_c = 0.45$, the change from the $\mu = 0$ value of the pressure is about 4%. At the RHIC $\mu/T_c = 0.15$, and the change in pressure is negligible.

The equation of state is the relation between the pressure and the quark number density at a fixed temperature. This is shown for the high temperature phase after taking the quenched continuum limit in figure 7. Deviations from a simple power law become visible only when the number density becomes of order T^3 . The slope of the equation of state also shows a power law behaviour for small n/T^3 .

In QCD with dynamical quarks, the equation of state has been obtained at cut-off of $a = 1/4T$ in [8,21,36] as a by-product of the identification of the critical end-point. The continuum limit has not yet been approached in any of these computations.

4.3 Strangeness production rates

Another piece of phenomenology that can be derived from Taylor expansion coefficients is the relative rate of strange and light quark production. In thermal equilibrium, the rate of production of particles is obtained through linear response theory. Measurements of Euclidean correlation functions have been continued into particle production rates using Bayesian techniques to extract the spectral functions needed for the analytic continuation [37]. It is possible to simplify the ratio of total quark production rates, if one assumes a relaxation time approximation for the spectral functions. Making further assumption that the relaxation time is longer than the (inverse) masses of the quarks, one finds that the ratio of the production rates is the ratio of the quark number susceptibilities [38].

If the fireball produced in heavy-ion collisions is initially gluon dominated, then, λ_s , the so-called Wroblewski parameter, i.e., the ratio of newly produced strange to

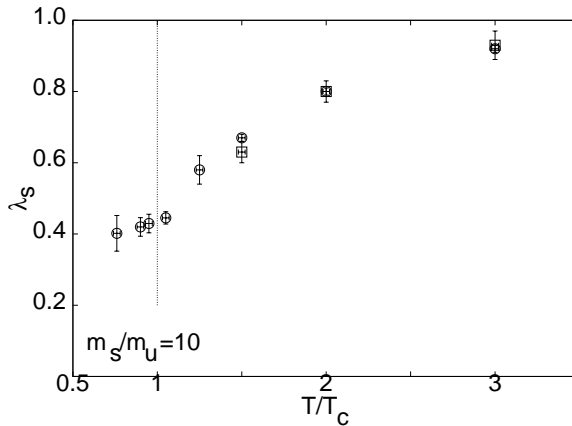


Figure 8. The relative rates of strange and light quark pair production as a function of temperature in QCD with two flavours of light sea quarks at lattice cut-off $a = 1/4T$ (circles) and quenched QCD in the continuum limit (squares). The light quark mass has been tuned to give $m_\pi/T_c = 1.6$ [21]. The rate of change with respect to the light quark mass can be obtained using the information in figure 6.

light quark pairs, is exactly the same as the ratio of the corresponding production rates. If, on the other hand, there is a degree of chemical equilibration, then the two ratios begin to differ by an amount that corresponds to the backward reaction rate. In figure 8 we show an estimate of the ratio of strange and light quark production rates computed in QCD at finite lattice spacing as a function of T . Also shown is the same ratio computed in quenched QCD in the continuum limit. In ratios such as this, lattice artifacts tend to cancel out.

Perhaps the severest source of lattice uncertainty here is the effect of the light quark masses on the ratio of the rates [34,39], as can be estimated from the mass dependence shown in figure 6. Future lattice computations need to take this into account by going towards realistic strange and light quark masses. Other uncertainties in the argument which need to be checked are detailed in [38].

5. Conclusion

I have reported three different methods which were developed recently in order to explore the phase diagram of QCD through lattice simulations. At least two of these seem to be general purpose methods to evade the fermion-sign problem partially. I examined these methods in §2 and applied them to the evaluation of simple integrals.

With the development of these methods it becomes possible to extend computations of QCD thermodynamics out to non-vanishing baryon density and accurately examine theoretical aspects of ongoing experimental work such as event-to-event fluctuations in conserved quantities, and the equation of state. It also becomes possible for the first time to examine strangeness production rates. I have touched upon these topics in §4.

One of the most promising developments is the possibility that one may begin to tie down theoretical speculations about the phase diagram of QCD – especially the position of the critical end-point. I have summarized the state of the art in this field in §3.

References

- [1] M G Alford, K Rajagopal and F Wilczek, *Phys. Lett.* **B422**, 247 (1998)
R Rapp, T Schafer, E V Shuryak and M Velkovsky, *Phys. Rev. Lett.* **81**, 53 (1998)
- [2] Since the internucleon force has an attractive component, pairing is possible also in nuclear matter, as was recognized long ago. See, for example, A de Shalit and H Feshbach, Theoretical nuclear physics, in *Nuclear Structure* (Wiley, New York, 1990) vol. 1. This has important consequences for spectroscopy and compact stars
- [3] M G Alford, K Rajagopal and F Wilczek, *Nucl. Phys.* **B537**, 443 (1999)
T Schäfer, *Nucl. Phys.* **B575**, 269 (2000)
- [4] P F Bedaque and T Schäfer, *Nucl. Phys.* **A697**, 802 (2002)
D B Kaplan and S Reddy, *Phys. Rev.* **D65**, 054042 (2002)
- [5] Z Fodor and S D Katz, *J. High Energy Phys.* **03**, 014 (2002)
- [6] C R Allton *et al*, *Phys. Rev.* **D66**, 074507 (2002)
- [7] R V Gavai and S Gupta, *Phys. Rev.* **D68**, 034506 (2003)
R V Gavai and S Gupta, *Nucl. Phys. Proc. Suppl.* **129**, 524 (2004)
- [8] C R Allton *et al*, *Phys. Rev.* **D68**, 014507 (2003)
- [9] M D’Elia and M P Lombardo, hep-lat/0209146
- [10] P De Forcrand and O Philipsen, *Nucl. Phys.* **B642**, 290 (2002)
- [11] ALADIN Collaboration: B Zwieglinski *et al*, *Nucl. Phys.* **A681**, 275 (2001)
- [12] D T Son and M A Stephanov, *Phys. Rev. Lett.* **86**, 592 (2001)
- [13] I M Barbour, *Nucl. Phys. Proc. Suppl.* **B60**, 220 (1998)
- [14] A sharper estimate is $N_s P(s_{\text{lim}}) = \sqrt{N_s}$, giving $s_{\text{lim}}^{\text{Gaussian}} = \sqrt{\sigma/2} \log(N_s/2\pi\sigma)$. For the numerical example in figure 4 this yields $s_{\text{lim}}^{\text{Gaussian}} = 3.58$, which is significantly closer to the observation
- [15] A M Ferrenberg, D P Landau and R H Swendsen, *Phys. Rev.* **E51**, 5092 (1995)
- [16] While the leading Taylor coefficients, i.e., the quark number susceptibilities, were first investigated in [17], the first systematic use of the Taylor expansion was to examine shifts in hadron masses at finite μ [18]
- [17] S Gottlieb *et al*, *Phys. Rev. Lett.* **59**, 2247 (1987)
- [18] S Choe *et al*, *Phys. Rev.* **D65**, 054501 (2002)
- [19] P Giudice and A Papa, *Phys. Rev.* **D69**, 094509 (2004)
- [20] S Gupta, *Phys. Lett.* **B588**, 136 (2004)
- [21] R V Gavai and S Gupta, in preparation
- [22] Z Fodor and S D Katz, *J. High Energy Phys.* **02**, 050 (2004)
- [23] S Gottlieb *et al*, *Phys. Rev.* **D38**, 2245 (1988)
- [24] A Peikert, Ph.D. Thesis, University of Bielefeld, May 2000
<ftp://ftp.uni-bielefeld.de/pub/papers/physik/theory/e6/dissertationen/peikert.ps.gz>
- [25] Y Iwasaki *et al*, *Phys. Rev. Lett.* **67**, 3343 (1991)
G Boyd *et al*, *Nucl. Phys.* **B469**, 419 (1996)
- [26] I have not discussed estimates of the curvature of the transition line near the critical end point. This has been estimated in [8,10]. See the talk of C Schmidt in SEWM 2004 (Helsinki) for more on this topic (http://www.physics.helsinki.fi/tfo_sewm/slides/schmidt/)

- [27] M Asakawa, U Heinz and B Müller, *Phys. Rev. Lett.* **85**, 2072 (2000)
S Jeon and V Koch, *Phys. Rev. Lett.* **85**, 2076 (2000)
- [28] R V Gavai and S Gupta, *Phys. Rev.* **D64**, 074506 (2001)
- [29] R V Gavai and S Gupta, *Phys. Rev.* **D67**, 034501 (2003)
- [30] J-P Blaizot, E Iancu and T Rebhan, *Phys. Lett.* **B523**, 143 (2001)
- [31] A Vuorinen, *Phys. Rev.* **D68**, 054017 (2003)
- [32] F Karsch, K Redlich and A Tawfik, *Phys. Lett.* **B571**, 67 (2003)
- [33] The MILC Collaboration: C Bernard *et al*, hep-lat/0405029
- [34] S Gupta and R Ray, in preparation
R V Gavai, S Gupta and R Ray, nucl-th/0312010
- [35] J Cleymans, *J. Phys.* **G28**, 1575 (2002)
- [36] Z Fodor, S Katz and K K Szabo, *Phys. Lett.* **B568**, 73 (2003)
- [37] F Karsch *et al.*, *Phys. Lett.* **B530**, 147 (2002)
S Gupta, hep-lat/0301006
- [38] R V Gavai and S Gupta, *Phys. Rev.* **D65**, 094515 (2002), hep-ph/0403172
- [39] O Miyamura *et al*, *Phys. Rev.* **D66**, 077502 (2002)